Manufacturing Science and Education 2025

ACTA TECHNICA NAPOCENSIS

Series: Applied Mathematics, Mechanics, and Engineering
Vol. 68, Issue Special II, Month July, 2025

STUDY OF STRAINS AND FORCES IN THE INCREMENTAL FORMING OF CLAD MATERIAL AL 3003/AL 4343

Robert-Marian BLEOTU, Sever-Gabriel RACZ, Cosmin PREDA, Eugen AVRIGEAN

Abstract: *This article investigates the formability of aluminum-clad materials during the Single Point Incremental Forming (SPIF) process. Clad materials have become an important choice in the automotive and aerospace industries due to their unique combination of mechanical and functional properties provided by distinct aluminum alloy layers. In the experiments, a clad material consisting of an Al 3003 substrate and an Al 4343 clad layer was used. The study focuses on the analysis of deformations and forces required during the SPIF process applied to this type of material. Experimental tests were conducted using an ARAMIS optical measurement system, a force measurement system, and an industrial robot to ensure process accuracy. Additionally, the chemical composition of each clad layer was determined using the HELIOS HYDRA (SEM) dual-beam electron microscope, providing a detailed characterization of the material. The results of this study contribute to a better understanding of the behavior of clad materials in the incremental forming process.*

Keywords: *incremental forming, cladded materials, deformation forces, Al3003/Al4343, chemical composition.*

1. INTRODUCTION

In the contemporary engineering market, a primary focus on energy efficiency, durability and performance optimization has catapulted lightweight materials into the spotlight. Industries such as aerospace, automotive, biomedical and consumer electronics are looking for ways to reduce component weight without compromising structural integrity or functionality. Lightweight materials, particularly aluminum, magnesium, titanium alloys and advanced composites, are usually used. These materials are characterized by very high strength-to-weight, corrosion resistance and thermal properties suitable for weight-sensitive applications [1]. However, from these materials, complex geometries are manufactured by traditional forming methods such as stamping or deep drawing, which involve high tooling costs, long lead times and limited flexibility. As a result, attention has been directed towards alternative processes, with incremental sheet forming (ISF) supposed to be the precursor, even if "ISF process has been researched in the last 20 years with limited applications in industries", because of geometrical accuracy, finishing surface [2-4].

Incremental sheet metal forming, with its significant flexibility, has recently been introduced and is attracting attention for creating complex shapes without molds. Prototype and small-batch production benefit most from this process, which minimizes tooling costs and lead times "compared to conventional forming techniques such as stamping or deep drawing" [5].

Defined by localized deformation, ISF works by using a small numerically controlled tool along a prescribed path to gradually deform the sheet into the desired shape. The method has a wide range of application potential, especially with the new lightweight alloys and bimaterials that are becoming increasingly important in applications such as aerospace, automotive, and biomedical engineering [6].

Incremental sheet metal forming is a forming method by which the surface of the sheet metal is machined even under CNC conditions and progress. The forming method "can be broadly divided into two types, namely, single-point incremental forming and two-point incremental forming" [7]. In SPIF, "the sheet is clamped on its edges and, with a single forming tool", is subsequently moved and deformed. In contrast, in TPIF, some kind of secondary support is introduced to provide better control over the geometry of the formed part and to improve its accuracy [8]. Most of the research in the specialized literature has been based on the influence of tool rotational speed [9], feed rate [10], toolpath [11], material type, and tool geometry [12] on the formability of the workpiece and the optimization of the ISF process [13].

To gain a better understanding of material behavior during the ISF process, numerous studies have been conducted to analyze strain distribution [14, 15]. It has been found that a detailed knowledge of this distribution not only allows for the evaluation of fracture mechanisms in incremental forming but also enables the determination of material formability [16]. The most effective method for measuring strains in ISF is the non-contact optical technique, which allows real-time monitoring throughout the entire process [17, 18].

Another essential parameter of the SPIF process is the evolution of forces during forming. This aspect has attracted significant interest among researchers since, in this process, the forming forces are considerably lower compared to traditional methods such as deep drawing [19]. A disadvantage of the SPIF process, compared to conventional methods, is that designers cannot preselect the deformation forces. For this reason, researchers are looking for solutions to determine and estimate the forming forces [20]. Establishing these forces in advance is crucial for optimizing the process, enabling the correct selection of parameters and the appropriate forming equipment. If the forces exceed the allowable limits, they can negatively impact product quality, tool rigidity, the clamping system, and the performance of the forming equipment [19].

In the SPIF process, due to the presence of intense and localized deformation, significant friction forces occur at the tool-workpiece interface. Most of the reviewed studies analyze only the force in the vertical direction (Oz), while neglecting the other two horizontal components (Ox and Oy). However, it is essential to investigate their influence as well, since the generated stresses can impact the performance and durability of the equipment used in the SPIF process [21].

Since lightweight materials are highly sought after in most industries, numerous studies have been conducted on materials such as aluminum alloy sheets [22, 23], copper alloys [24, 25], magnesium alloys [26, 27], and titanium alloys [28, 29].

In addition to the interest in alloys made from lightweight materials, a highly relevant and current topic is the study of bimetallic materials. These materials offer the major advantage of having distinct properties on each of their surfaces [30]. However, although bimetals have significant potential, research on their behavior in the ISF process remains limited. The specialized literature includes studies on bimetallic materials such as Aluminum/Copper [31-33], Steel/Titanium [34], and Aluminum/Steel [35].

Another category of materials used in the automotive and aerospace industries is clad materials [36]. In the aerospace industry, aircraft fuselages are made from high-strength aluminum alloys; however, a major drawback of these materials is their low corrosion resistance. An effective solution to this problem is the use of clad materials. In this case, the base material consists of a high-strength aluminum alloy, while the cladding layer is made from an aluminum alloy with high corrosion resistance [37].

This study aims to make a significant contribution to understanding the behavior of clad materials following the SPIF process. The main objective is to analyze the deformations and forces generated during this process.

2. MATERIALS AND METHODS

2.1 Materials

This research utilized a 1.2 mm thick clad material, consisting of a base material (EN AW 3003) and an upper cladding material (EN AW 4343). To highlight the layered structure of this material used in the experiment, Figure 1 presents its 3D representation.

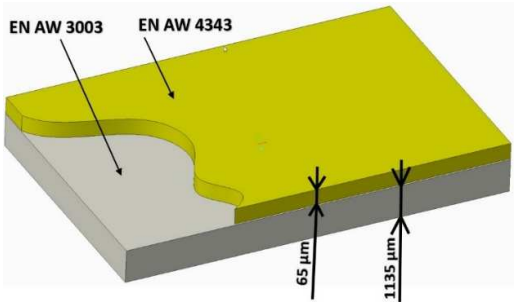

Fig. 1. 3D Diagram – Clad Material.

This type of clad material is specifically designed for use in the automotive industry, particularly in the production of radiators, due to its excellent heat transfer properties. Thus, the EN AW 3003 alloy is chosen for its good mechanical properties, thermal conductivity, and corrosion resistance. The clad material, EN AW 4343, is used in the brazing process due to its high silicon content and also serves as a protective layer against corrosion.

To observe the contact interface between the two materials and measure their thickness, the dual-beam microscope HELIOS HYDRA (SEM) was used, as illustrated in Figure 2. To highlight the structural differences between the two aluminum alloys, the backscattered electron detector of the SEM microscope was used in Z-contrast mode.

In order to obtain the most precise images, the sample required prior preparation. After the sample was cut using a diamond disc-equipped cutting machine with cooling assistance (Struers Labotom-5), it was embedded in resin (ClaroCit Powder and ClaroCit Liquid) and placed in a pressure pot for 30 minutes at a temperature of 80˚C. After this step, the embedded sample was polished using abrasive discs (500, 1000, 1200, and 2000 grit). In the final preparation step, the sample was polished with the DiaPro MOL E 3 µm solution (special solution for polishing aluminum alloys). It is also important to mention that, due to the sample grinding and polishing process, chemical elements can easily migrate from one layer to another. Consequently, the analysis results may be influenced to some extent.

Fig. 2. SEM Microscope Used for the Microstructural Analysis of the Clad Material.

As observed in Figure 3, the thickness of the cladded layer (EN AW 4343) has an average value of 66.78 µm. Accordingly, the thickness of the base layer has an average value of 1133.22 µm.

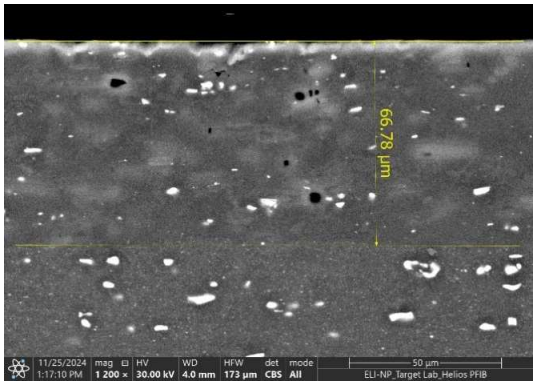

Fig. 3. Interface and Cladding Layer Measurement.

In addition to the microstructural analysis, the SEM microscope equipped with an Energy Dispersive Spectroscopy (EDS) detector was also used to determine the chemical composition of the two different aluminum alloys. For higher measurement accuracy, the layers were scanned in the longitudinal direction. This avoided the separation zone between the two aluminum alloys that form the cladded material. The scan was performed over an area of approximately 500 µm x 70 µm. Figure 4 and Figure 5 show the EDS spectra obtained for the two types of aluminum alloys used in the study. The spectra highlight the chemical composition of the base

material (EN AW 3003) and the cladded layer (EN AW 4343). As a result, a high concentration of silicon (17.15%) in the cladded layer is observed, compared to the base layer (0.66%).

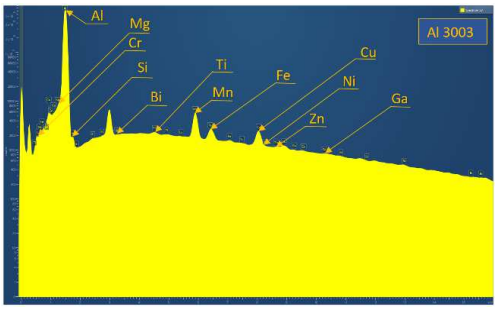

Fig. 4. EDS Spectrum – Al 3003.

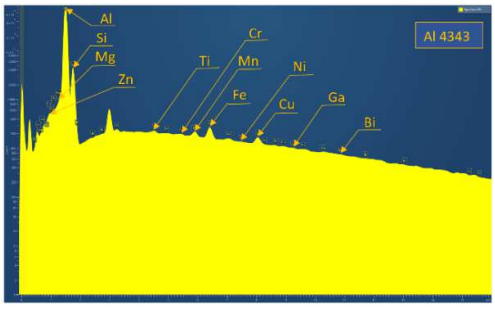

Fig. 5. EDS Spectrum – Al 4343.

In order to obtain the most precise results, five measurements were taken in different areas of the longitudinal surface of the analyzed sample. The obtained data were then statistically processed to verify the normal distribution and to eliminate any outliers. For this purpose, the Anderson-Darling test was applied. To limit the number of graphs presented, Figure 6 shows only the statistical distribution of the chemical element that differentiates the two aluminum alloys, namely silicon.

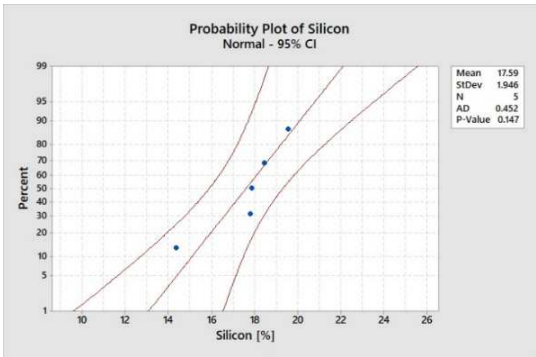

Fig. 6. Probability Plot Graph – Silicon.

From the obtained graphs, we observed that the AD value for the measured chemical elements is relatively small (0.452 for silicon), which suggests that the deviation from the normal distribution is not significant. Additionally, the p-value exceeds the 0.05 threshold, allowing us to conclude that the measurements follow a normal distribution and that there are no outliers.

Table 1 presents the average chemical composition obtained from the measurements performed.

Table 1

Chemical Composition.

Chimical elements [%]	EN AW 3003	**Chimical elements** [%]	EN AW 4343
Mn	1,27	Si	17,15
Cu	0,67	Cu	0,22
Si	0,66	Fe	0,22
Fe	0,25	Mg	0,21
Mg	0,2	Mn	0,1
Ti	0,05	Ti	0,04
Bi	0,04	Zn	0,03
Zn	0,03	Bi	0,01
Ni	0,02	Ni	0,01
Al	Restul	Al	Restul

2.2 Incremental Sheet Forming

The main goal of the experimental research was to measure the deformations and the forces required for their application during the SPIF process. To manufacture a conical part, the SPIF process was carried out with the help of the KUKA KR 210-2 industrial robot. This is a 6-axis robot that can develop a maximum force of 2100 N and is equipped with a KR C2 control device.

After creating the 3D model in CATIA V5, it was imported into the SprutCam program. This program allowed for the creation of a spiral-type trajectory, necessary to form the geometry of a truncated cone. The geometry and its dimensions can be observed in Figure 7. The tool used in the process had a diameter of 10 mm.

The blank used in the SPIF process had a size of 240 x 240 mm. It was positioned vertically with the help of a special fixture.

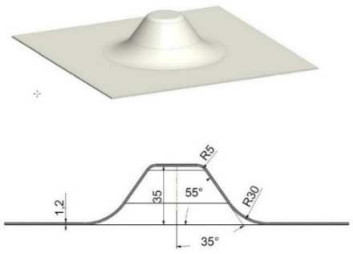

Fig. 7. Part Geometry and Dimensions.

For measuring the deformations, the ARAMIS optical measurement system was used. The equipment used in the SPIF process consisted of: ARAMIS software, optical cameras, clamping system, 6-axis robot, and robot controller. These components can be seen in Figure 8.

For force measurement during the SPIF process of clad materials, a measurement system was used, consisting of the "PCB261A13 sensor (PCB Piezotronics, Depew, NY, USA), the CMD600 signal amplifier (HBM, Darmstadt, Germany), and the Quantum X MX840B data acquisition system (HBM, Germany)". The PCB261A13 sensor, mounted on the robot arm, was used to monitor the forces generated during the forming process.

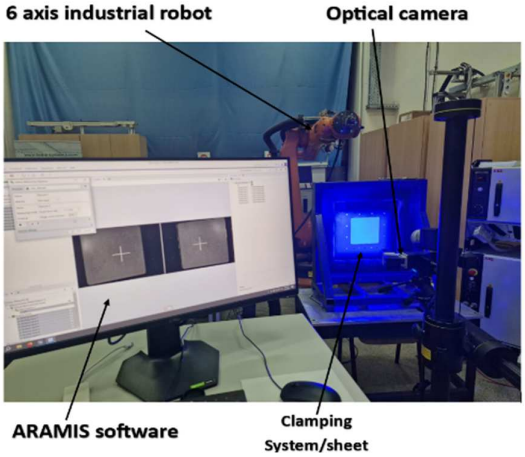

Fig. 8. Equipment Used in the SPIF Process.

In order to carry out the experimental investigations, a single incremental forming test was performed, with the objective of analyzing the material behavior under the action of the forces applied during the SPIF process. The decision to conduct only one test is justified by the preliminary nature of the study, which focuses on validating the measurement method and highlighting the main phenomena characteristic of the analyzed process.

Additionally, the test monitored the behavior of the interface between the cladded layer and the base material, with the aim of identifying any potential delamination phenomena resulting from the SPIF process.

3. RESULTS

3.1 Deformation State Analysis

Following the SPIF process, where the Kuka KR210-2 industrial robot was used, the main strains were measured, including: strain along the X-axis (εx), strain along the Y-axis (εy), major strain (ε1), secondary strain (ε2), equivalent Von Mises strain (εVM), and shear strain (εxy). Using the clamping device, the blank was positioned so that the base material was oriented on the side opposite to the contact surface with the forming tool. In this configuration, optical cameras were employed to measure the deformations resulting from the SPIF process.

The forming operation was performed relative to the coordinate system of the robotic arm, where the Z-axis is defined as being perpendicular to the plane of the blank. This orientation was used both for accurate positioning of the forming tool and for interpreting the displacements and forces recorded during the process. The resulting part, shaped as a conical frustum, is shown in Figure 9.

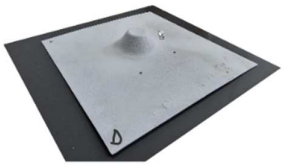

Fig. 9. The conical frustum part.

The sequence of Figure 10, Figure 11, Figure 12, Figure 13, Figure 14 and Figure 15 present the actual experimental results obtained for the principal strains following the SPIF process. Additionally, Table 2 provides a summary of these results.

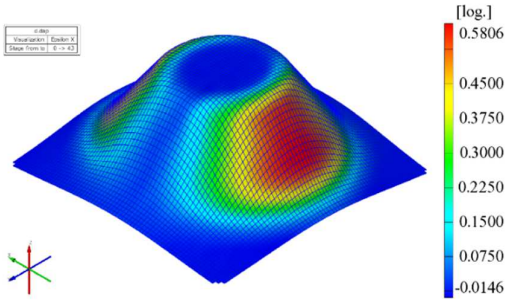

Fig. 10. Distribution Along the X-Axis (ε_x).

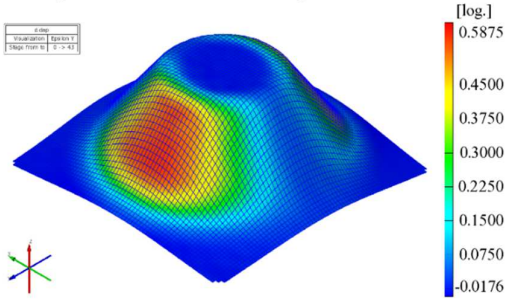

Fig. 11. Distribution Along the Y-Axis (ε_y).

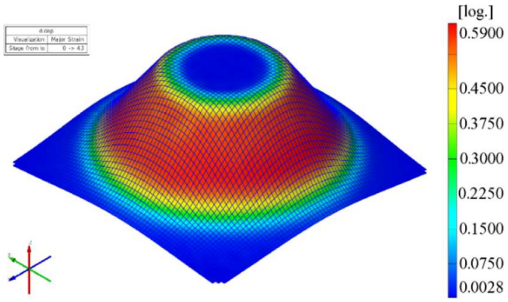

Fig. 12. Major strain (ε_1).

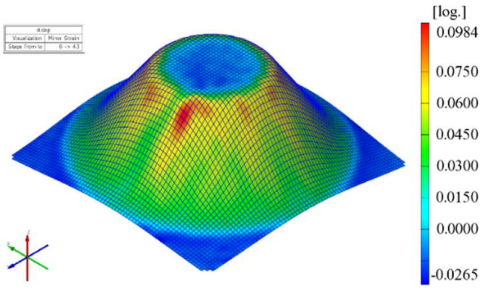

Fig. 13. Minor strain (ε_2).

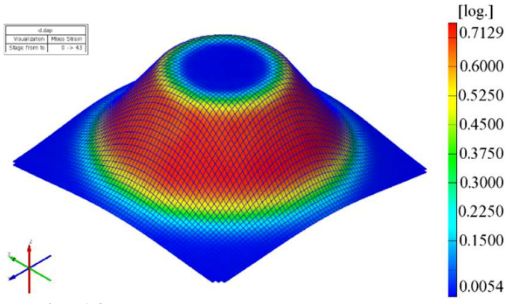

Fig. 14. Von Mises Equivalent Strain (ε_{VM}).

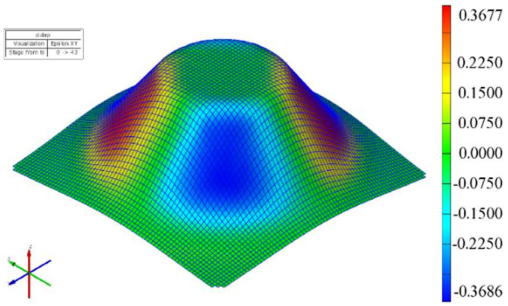

Fig. 15. Shear Strain (ε_{xy}).

Table 2

Results obtained for strain measurements.

Strain	Measured value [mm/mm]
ε_x	0,5806
ε_y	0,5875
ε_1	0,5900
ε_2	0,0984
ε_{VM}	0,7129
ε_{xy}	0,3677

Based on the results obtained, it can be observed that, in the case of deformations ε_x and ε_y, their maximum values are located along the respective axes (the Ox axis, respectively the Oy axis). Given that the values for the two deformations are close in magnitude, we can conclude that the deformation occurs symmetrically throughout the process. The same conclusion can be applied to the deformation $^{\varepsilon xy}$.

Regarding the distribution of the major strain, it is observed that the maximum values are concentrated in the truncated cone region, with a local peak at its large base. In the case of the minor strain, the maximum values are radially distributed around the small base of the truncated cone.

The Von Mises equivalent strain shows a distribution similar to the major strain, but with a higher maximum value.

To provide a complete description of the material behavior throughout the SPIF process, both the displacement along the Z-axis (the tool advancement axis) and the shear angle were considered. The values obtained for these two variables are presented in Figure 16 and Figure 17. The maximum displacement value along the Oz axis is 34.6 mm, located at the small base of the truncated cone. As for the maximum shear angle value, it is 29.15° and is found in the truncated cone region.

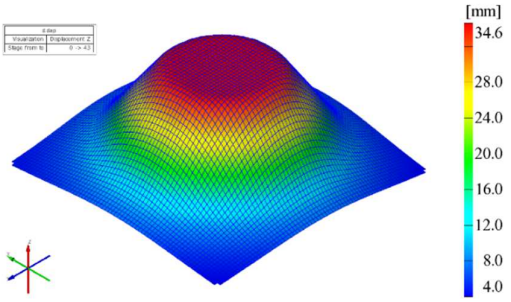

Fig. 16. Displacement along the Oz axis.

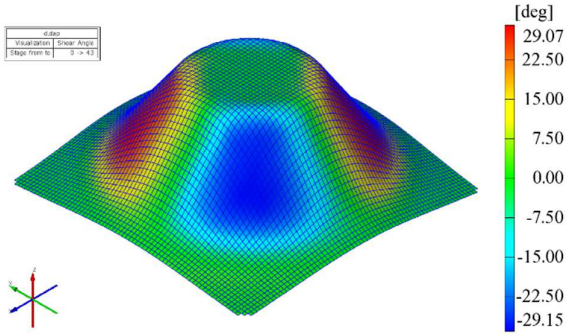

Fig. 17. Shear angle.

3.2 Determination of Forces During the SPIF Process

One of the most important output parameters in the SPIF process is the force developed during the process. Unlike conventional processes (e.g., deep drawing), the force developed in the SPIF process consists of three components that vary throughout the process. Therefore, measuring the forces during the SPIF process of the clad material required the use of a force sensor, a conditioning module, and a data acquisition system. Figure 18, Figure 19 and Figure 20 present representative graphs for the three directions of the axis system.

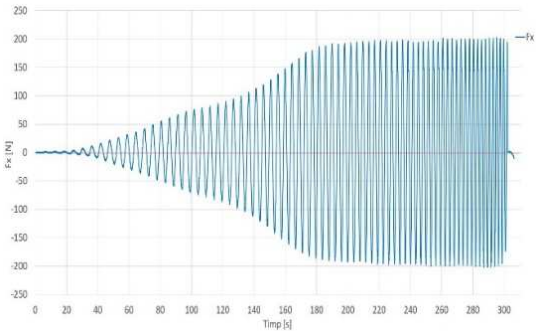

Fig. 18. The Fx force variation.

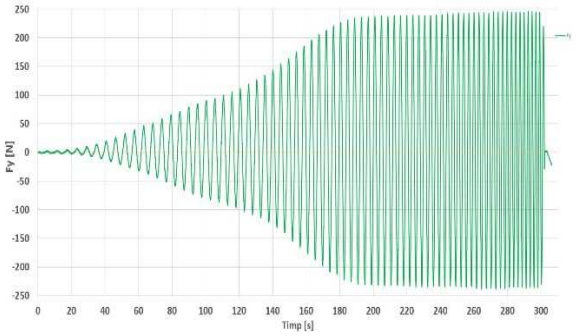

Fig. 19. The Fy force variation.

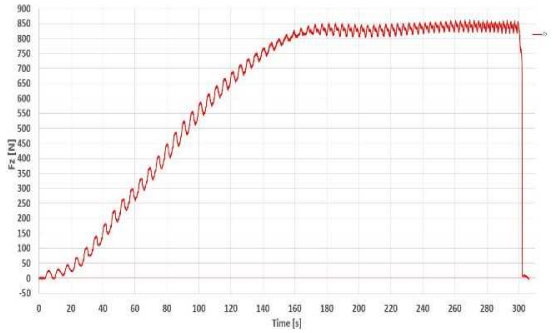

Fig. 20. The Fz force variation.

From the graphs obtained for the variation of forces along the three directions, it can be observed that the force along the X direction and the force along the Y direction increase from a value of 0 at the beginning of the process to the maximum value observed at the end of the process. These forces exhibit a sinusoidal variation, oscillating around zero. Additionally, small variations can be observed along the way, which is due to the position of the punch. The maximum value along the X direction is 202.21 [N], while the maximum value along the Y axis is 246.50 [N].

In the case of the force along the Z axis (perpendicular to the table plane), the values are positive throughout the process, which is due to the punch's advancing direction. The maximum value is 861.97 [N], which occurs at the end of the process. It can also be observed that Fz is much larger than Fx and Fy, making it a more significant force, as it directly affects the magnitude of the resultant force at the apex.

3.3 Visual Inspection for Delamination After the SPIF Process

Following the visual inspection of the formed part, no signs of delamination were observed at

the interface between the cladded layer and the base material. Figure 15 shows a detailed image of the material surface, captured from the conical part area, where local stresses are higher. The image confirms that the layered structure remained intact, with no evidence of peeling, cracking, or separation zones.

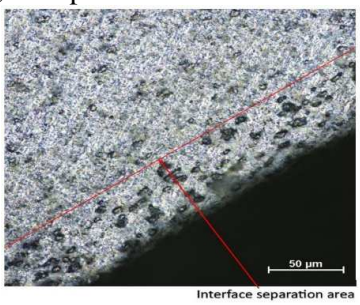

Fig. 21. Visual detail of the layered interface in the high-stress zone.

4. CONCLUSION

The main objective of this paper was to determine the deformations and forces that occur during the SPIF process applied to plated materials. Based on the study conducted, it was found that the plated material withstands the SPIF process without the layers delaminating. Additionally, it was observed that the chemical composition plays an important role in the behavior of these types of materials.

From the perspective of the deformations studied during the SPIF process, it was found that, due to the values obtained for the εx and εy deformations, the deformation process occurs symmetrically. The area with the highest stresses is located in the conical frustum region, with a local peak at its large base, while the minor strain is radially distributed at the small base of the conical frustum.

Following the force analysis, it was concluded that, due to the values obtained for Fx and Fy, the deformation is symmetric. However, considering the significantly larger value of the Fz force, it can be concluded that it represents the main force in the process, having a major influence on it.

This research provides an experimental basis for future studies focused on optimizing SPIF process parameters for cladded or similar materials, as well as for the development of advanced methods for controlling and predicting the behavior of layered structures during plastic deformation.

5. REFERENCES

[1] Dylan, P., David, R., Marco, G., Gianluca, B., Livan, F., Hitomi, Y., *Study of forming mechanics of magnetic field–assisted single point incremental forming*, Journal of Manufacturing Processes, ISSN 1526-6125, 79, 28-34, 2022.

[2] Trzepieciński, T., Najm, S.M., Pepelnjak, T., Bensaid, K., Szpunar, M., *Incremental Sheet Forming of Metal-Based Composites Used in Aviation and Automotive Applications*, Journal of Composites Science, 6(10):295, 2022.

[3] Lu, B., Fang, Y., Xu, D, Chen, J., Ou, H., Moser, N.H., Cao, J., *Mechanism investigation of friction-related effects in single point incremental forming using a developed oblique rolled-ball tool*, International Journal of Machine Tools & Manufacture, ISSN 0890-6955, 85, 14-29, 2014.

[4] Kumar, A., Gulati, V., Kumar, P., *Effects of Process Parameters on Surface Roughness in Incremental Sheet Forming*, Materials Today: Proceedings, ISSN 2214-7853, 5, 14, 2018.

[5] Ullah, S., Xu, P., Li, X., Li, Y., Han, K, Li, D., *A Review on Part Geometric Precision Improvement Strategies in Double-Sided Incremental Forming*, Metals, 12(1):103, 2022.

[6] Emami, M., Morovvati, M., Mollaei-Dariani, B., Arezoodar, A.F., *Investigation of the formability of Al1050/DC01 bi-layer sheet in incremental hole-flanging: Experimental and numerical simulation*, European Journal of Mechanics / A Solids, 30, 71-76, 2019.

[7] Trzepieciński, T., Oleksik, V., Pepelnjak, T., Najm, SM, Paniti, I., Maji, K., *Emerging Trends in Single Point Incremental Sheet Forming of Lightweight Metals*, Metals, 11(8), 1188, 2021.

[8] Trzepieciński, T., Oleksik, V., Pepelnjak, T., Najm, SM, Paniti, I., Maji, K., *Emerging Trends in Single Point Incremental Sheet Forming of Lightweight Metals*, Metals, 11(8), 1188, 2021.

[9] Azpen, Q., Beharudin, H., Sulaiman, S., Mustapha, F., *Effect of process parameters on the surface roughness of aluminum alloy AA 6061-T6 sheets in frictional stir incremental forming*, Advances in Production Engineering & Management, 13(4):405-416, 2018.

[10] Baruah, A., Pandivelan, C., Jeevanantham, A.K., *Optimization of AA5052 in incremental sheet forming using grey relational analysis*, Measurement, 106, 95–100, 2017.

[11] Wu, S.H., Reis, A., Andrade Pires, F.M., Santos, A.D.; Barara da Rocha, A. *Study of tool trajectory in incremental forming*, Advanced Materials Research, 472, 1586–1591, 2012.

[12] Jeswiet, J., *Asymmetric Incremental Sheet Forming*, Advanced Materials Research, 6–8 ,35–58, 2005.

[13] Skjoedt, M., Bay, N., Endelt, B., Ingarao, G., *Multi-step strategies for incremental single-point formation of a cup. International*, International Journal of Material Forming, 1:1199-1202, 2012.

[14] Amala Justus Selvam, M., Velu, R., Dheerankumar, T., Study of the influence of the process variables on formability and strain distribution in incremental sheet metal working of AA 1050 sheets, n Lecture Notes in Mechanical Engineering, ISBN 978-981-10-1771-1, 493–505, 2017.

[15] Kumar, G., Maji, K., Investigations on formability of tailor laminated sheets in single point incremental forming, Proc. Inst. Mech. Eng. Part B J. Eng. Manuf., 236(10):1393-1405, 2022.

[16] Raju, C., Haloi, N., Narayanan, S., Strain distribution and failure mode in single point incremental forming (SPIF) of multiple commercially pure aluminum sheets, Journal of Manufacturing Processes, ISSN 1526-6125, 30, 328-335, 2017.

[17] Mugendiran, V., Gnanavelbabu, A., Comparison of plastic strains on AA5052 by single point incremental forming process using digital image processing, J. Mech. Sci. Technol., 31, 2943–2949, 2017.

[18] Vanhulst, M., Vanhove, H., Carette, Y., Waumans, S., Duflou, J.R., Analysis of Thickness Distributions Calculated from Surface Strains Obtained through Digital Image Correlation for Incremental Sheet Forming, In Key Engineering Materials, 926, 875–882, 2022.

[19] Baharudin, B.T.H.T., Azpen, Q.M., Sulaima, S., Mustapha, F., Experimental Investigation of Forming Forces in Frictional Stir Incremental Forming of Aluminum Alloy AA6061-T6, Metals, 7(11), 484, 2017.

[20] Al-Ghamdi, K.A., Hussain, G., Forming forces in incremental forming of a geometry with corner feature: investigation into the effect of forming parameters using response surface approach, Int J Adv Manuf Technol, 76, 2185–2197, 2015.

[21] Rosca, N., Trzepieciński, T., Oleksik, V., Minimizing the Forces in the Single Point Incremental Forming Process of Polymeric Materials Using Taguchi Design of Experiments and Analysis of Variance, Materials, 15(18):6453, 2022.

[22] Kumarab, A.; Gulati, V.; Kumar, P.; Singh, V.; Kumar, B.; Singh, H., *Parametric effects on formability of AA2024-O aluminium alloy sheets in single point incremental forming*, J. Mater. Res. Technol., 8, 1461–1469, 2019.

[23] Choudhary, S., Mulay, A., *Influence of Tool Size and Step Depth on the Formability Behavior of AA1050, AA6061-T6, and AA7075-T6 by Single-Point Incremental Forming Process*, J Mater Eng Perform, 33, 3283-3298, 2024.

[24] Fratini, L., Ambrogio, G., Di Lorenzo, R., Filice, L., Micari, F., *Influence of mechanical properties of the sheetmaterial on formability in single point incremental forming*, CIRP Ann., 53, 207–210, 2004.

[25] Fritzen, D., Daleffe, A., do Santos De Lucca, G, Castelan, J., Schaeffer, L., *Incremental forming of Cu-35Zn brass alloy*, International Journal of Material Forming, 11, 389-404, 2018.

[26] Zhang, Q., Xiao, F., Guo, H., Li, C., Gao, L., Guo, X., Han, W., Bondarev, A.B., *Warm negative incremental forming of magnesium alloy AZ31 sheet: New lubricating method*, J. Mater. Process. Technol., 210, 323-329, 2010.

[27] Cusanno, A., Negrini, N.C., Villa, T., Farè, S., Garcia-Romeu, M.L., Palumbo, G., *Post*

Forming Analysis and In Vitro Biological Characterization of AZ31B Processed by Incremental Forming and Coated with Electrospun Polycaprolactone, ASME. J. Manuf. Sci. Eng., 143, 011012, 2021.

[28] Gottmann, A., Diettrich, J., Bergweiler, G., Bambach, M., Hirt, G., Loosen, P., *Laser assisted asymmetric incremental sheet forming of titanium sheet metal parts*, Prod. Eng., 5, 263–271., 2011.

[29] Thakur, S., Chauhan, S.R., *Development of a Critical Edge-Based Adaptive Toolpath Strategy to Improve Geometrical Accuracy of Incrementally Formed Titanium Implants*, Journal of Manufacturing Processes, ISSN 1526-6125, 2024.

[30] Zaba, K., Puchlerska, S., Kuczek, L., Trzepieciński, T., Maj, P. *Effect of Step Size on the Formability of Al/Cu Bimetallic Sheets in Single Point Incremental Sheet For-ming.*, Materials, 16, 367, 2023.

[31] Gheysarian, A., Honarpisheh, M., *Process Parameters Optimization of the Explosive-Welded Al/Cu Bimetal in the Incremental Sheet Metal Forming Process.*, J. Sci. Technol. Trans. Mech. Eng., 43, 945–956, 2019.

[32] Honarpisheh, M., Mohammadi, J.M., Alinaghian, I., *Multi-response optimization on single-point incremental forming of hyperbolic shape Al-1050/Cu bimetal using response surface methodology*, Int. J. Adv. Manuf. Technol., 96, 3069–3080, 2018.

[33] Liu, Z.; Li, G., *Single point incremental forming of Cu-Al composite sheets: A comprehensive study on deformation behaviors*, Arch. Civ. Mech. Eng., 19, 484–502, 2019.

[34] Sahtemanian, M.R., Honarpisheh, M., Amini, S., *A novel material modeling technique in the single-point incremental forming assisted by the ultrasonic vibration of low carbon steel/commercially pure titanium bimetal sheet*, Int. J. Adv. manuf. Tehnol., 102, 473–486, 2019.

[35] Abd Ali, R., Chen, W., Jin, K, Bao, Y., Hussein, A.W., *Formability and failure analyses of Al/SUS bilayer sheet in single point incremental forming*, Int J Adv Manuf Technol, 105, 2785–2798, 2019.

[36] Himagireesh, C., Ramji, K., Durga Prasad, K.G., Hari Kiran, V., *ulti-criteria decision model for selection of a material suitable to lightning strike protection in aerospace applications,* Mater. Today Proc., 59, 725–733, 2022.

[37] Zinonga, T., Binga, Z., Junb, J., Zhiqianga, L., Jianguob, L., *A study on the hot roll bonding of aluminium alloys,* Procedia Manuf., 50, 56–62, 2020.

STUDIUL DEFORMAȚIILOR ȘI A FORȚELOR ÎN DEFORMAREA INCREMENTALĂ A MATERIALUI PLACAT AL 3003/AL 4343

Rezumat: Acest articol a investigat formabilitatea materialelor placate din aluminiu în timpul procesului de deformare incrementală într-un singur punct (SPIF). Materialele placate au devenit o alegere importantă în industria auto și aerospațială datorită combinației lor unice de proprietăți mecanice și funcționale, oferite de straturile distincte de aliaje de aluminiu. În cadrul experimentelor, s-a utilizat un material placat format dintr-un substrat de Al 3003 și un strat placat de Al 4343. Studiul se concentrează pe analiza deformațiilor și a forțelor necesare în timpul procesului SPIF aplicat acestui tip de material. Testele experimentale au fost realizate utilizând un sistem optic de măsurare (ARAMIS), un sistem de măsurare a forțelor și un robot industrial pentru a asigura precizia procesului. În plus, compoziția chimică a fiecărui strat placat a fost determinată cu ajutorul microscopului electronic cu fascicul dual HELIOS HYDRA (SEM), oferind o caracterizare detaliată a materialului. Rezultatele acestui studiu contribuie la o mai bună înțelegere a comportamentului materialelor placate în procesul de deformare incrementală.

Robert-Marian BLEOTU, PhD Student, University Assistant, Lucian Blaga University of Sibiu, Machines and Industrial Equipment Department, robert.bleotu@ulbsibiu.ro, +4076101210.

Sever-Gabriel RACZ, Prof. Univ. Dr. Ing., Lucian Blaga University of Sibiu, Machines and Industrial Equipment Department, gabriel.racz@ulbsibiu.ro.

Cosmin PREDA, PhD Student, University Assistant, Lucian Blaga University of Sibiu, Machines and Industrial Equipment Department, cosmin.preda@ulbsibiu.ro.

Eugen AVRIGEAN, Assoc. Prof. Dr. Eng., Lucian Blaga University of Sibiu, Machines and Industrial Equipment Department, eugen.avrigean@ulbsibiu.ro.